Nanoscience and Nanometrology
2016; 2(2): 41-45
http://www.sciencepublishinggroup.com/j/nsnm
doi: 10.11648/j.nsnm.20160202.11
ISSN: 2472-3622 (Print); ISSN: 2472-3630 (Online)

Hydrothermal Synthesis Y_2O_3:Yb^{3+}/Er^{3+} Nanospheres with Upconversion Luminescence from Green to Red

Jie Yang, Jiali Gu, Renhe Yang, Qinyu Shang, Jun Yang*

School of Chemistry and Chemical Engineering, Southwest University, Chongqing, China

Email address:

65195828@qq.com (Jun Yang)

*Corresponding author

To cite this article:

Jie Yang, Jiali Gu, Renhe Yang, Qinyu Shang, Jun Yang. Hydrothermal Synthesis Y_2O_3:Yb^{3+}/Er^{3+} Nanospheres with Upconversion Luminescence from Green to Red. *Nanoscience and Nanometrology.* Vol. 2, No. 2, 2016, pp. 41-45. doi: 10.11648/j.nsnm.20160202.11

Received: September 29, 2016; **Accepted**: October 19, 2016; **Published**: November 3, 2016

Abstract: Well-dispersed, uniform Y_2O_3:Yb^{3+}/Er^{3+} nanospheres have been successfully prepared at 160°C *via* a facile hydrothermal route without using any templates, followed by a subsequent calcination process. X-ray diffraction, scanning electron microscopy, transmission electron microscopy, and upconversion photoluminescence spectra were employed to characterize the samples. The SEM and TEM images indicate that the samples consist of separated spheres with a mean diameter of about 75 nm. Under the excitation of 980-nm laser, the Y_2O_3:Yb^{3+}/Er^{3+} phosphors exhibit bright upconversion photoluminescence from green to red with different Yb^{3+} content, which is easily observed by our naked eyes. Due to multicolor tunable luminescence, ideal spherical shape, and cheap materials of Y_2O_3 host, the as-prepared phosphors are potentially applied for color displays, back light, UC lasers, photonics, and biomedicine.

Keywords: Y_2O_3 Nanosphere, Hydrothermal Synthesis, Yb→Er Energy Transfer, Upconversion Luminescence

1. Introduction

Inorganic luminescent materials with controllable and uniform size and shape have stimulated great interest because the morphology, dimensionality, and size of materials have great effect on their physical, chemical, magnetic, and catalytic properties as well as for their application in optoelectronic devices [1]. Much effort has been devoted to the fabrication of nanocrystals with various shapes [2], including zero-dimension (0D) isotropic spheres and cubes; 1D rods, wires, tubes, and belts; 2D plate, disk, and sheet; and 3D hierarchical architectures such as star, multipods, flowers, and dendrites. In particular, the ideal morphology of phosphor particles includes a perfect spherical shape, narrow size distribution, and nonagglomeration. Spherical morphology of the phosphors is good for high brightness and high resolution. Additionally, high packing densities and low scattering of light can also be obtained by using spherical phosphors [3]. So far, many synthetic routes have been developed to control the spherical shape, size, and distribution of phosphor particles, such as spray pyrolysis, sol-gel process, urea homogeneous precipitation, and template method [4-7].

Rare earth oxides have been extensively used in high performance luminescent devices, magnets, catalysts, and other functional materials because of their electronic, optical, and chemical characteristics resulting from the 4f electronic shells [8]. These properties depend strongly on the material chemical composition, crystal structure, shape, and dimensionality, which are sensitive to the bonding states of rare earth ions. In particular, due to their photophysical properties (such as low effective densities, low phonon energy, transparency to visual light), the Ln^{3+}-doped down-conversion (DC) and up-conversion (UC) rare earth oxides should be applied in drug/enzyme delivery, lightweight fillers, pigments, adsorption materials, specific phosphor powder, confined-space catalysis, and biomolecule release.

Among them, yttrium oxide (Y_2O_3) is a promising host matrix for down- and up-conversion luminescence, due to its good chemical durability, thermal stability, and low phonon energy. The rare earth ion Ln^{3+}-doped Y_2O_3 materials have been proven to be important down-conversion and up-conversion phosphors [9]. In particular, Y_2O_3:Ln^{3+} phosphor is a well-known phosphor that is used in fluorescent lights (FLs), field emission displays (FEDs), and cathode-ray tubes (CRTs), and luminescence in the three primary colors (RGB) through UC processes. Over the past decade, various

morphologies of Y_2O_3:Ln^{3+} have been synthesized via different methods [10], including nanoparticles through combustion, microemulsion, and chemical vapor technique; nanotubes fabricated by a surfactant assembly mechanism; nanowires induced by template-assisted growth in AAO; spherical particles by using spray pyrolysis method, urea homogeneous precipitation, and template method; and patterned thin films prepared from sol-gel soft lithography.

With the advantages of high purity, good homogeneity, high uniformity in particle size distribution and non-agglomeration, the hydrothermal synthesis method is an important "soft chemistry" technology for the preparation of low dimension nanostructures. Certainly, Y_2O_3:Ln^{3+} 1D structures induced by hydrothermal method have been reported [11]. However, to the best of our knowledge, few studies have focused on the synthesis of nanospherical Y_2O_3:Ln^{3+} through hydrothermal method without any template [10]. So, further investigations of spherical shape-controllable synthesis for Y_2O_3:Ln^{3+} together with their formation mechanisms via hydrothermal synthesis routes are still of great interest, which not only will be able to enrich the synthesis science, but also make it possible to find novel and improved properties of the existing materials.

Accordingly, in present work, we report the synthesis of uniform Y_2O_3:Yb^{3+}/Er^{3+} nanospheres using a hydrothermal process without any template followed by a further heat-treating. The structure, morphology, and formation process of the nanospheres have been well characterized by various analysis techniques. Under the excitation of 980-nm laser, the Y_2O_3:Yb^{3+}/Er^{3+} phosphors exhibit bright upconversion photoluminescence from green to red. The corresponding luminescent mechanisms have been discussed. Due to multicolor tunable luminescence, ideal spherical shape, and cheap materials of Y_2O_3 host, the as-prepared phosphors are potentially applied for color displays, back light, UC lasers, photonics, and biomedicine.

2. Experimental Section

2.1. Materials

The initial chemicals, including Y_2O_3, Yb_2O_3, and Er_2O_3 (all with purity ≥ 99.99%, Changchun Haipurui Rare Earth Materials Technology Co. Ltd., China), CH_3COOH, ethylene glycol, and ethanol (all with purity of A. R., Beijing Fine Chemical Company, China), were used without further purification.

2.2. Preparation

In a typical synthesis, stoichiometric (mol%) of Y_2O_3, Yb_2O_3, and Er_2O_3 were dissolved into dilute HAc, resulting in the formation of a colorless solution of $RE(Ac)_3$ (RE = Y, Yb, and Er). After evaporation followed by drying at 70°C for 10 h in ambient atmosphere, a powder of $RE(Ac)_3$ was obtained. Then ethylene glycol (38 mL) and H_2O (2 mL) were added to the powder of $RE(Ac)_3$. The solution was stirred for another 2.5 h. Then the transparent feedstock was introduced into a 50 mL Teflon-lined stainless autoclave and heated at 160°C for 24 h. After the autoclave was cooled to room temperature naturally, the precursors were separated by centrifugation, washing with ethanol and distilled water several times, and drying in atmosphere at 70°C for 5 h. The final products (Y_2O_3:Yb^{3+}/Er^{3+}) were retrieved through a heat treatment at 800°C in air for 4 h.

2.3. Characterization

The phase purity and crystallinity of the samples were examined by powder X-ray diffraction (XRD) performed on a Rigaku-Dmax 2500 diffractometer with Cu Kα radiation (λ = 0.15405 nm). The morphology and structure of the samples were inspected using a field emission scanning-electron microscopy (FE-SEM, XL 30, Philips). Transmission electron microscopy (TEM) images were performed using FEI Tecnai G2 S-Twinwere with a field emission gun operating at 200 kV. Images were acquired digitally on a Gatan multiple CCD camera. The UC photoluminescence emission spectra were obtained using 980 nm LD Module (K98D08M-30W, CHINA) as the excitation source and detected by R955 (HAMAMATSU) from 400 to 750 nm. All the measurements were performed at room temperature.

3. Results and Discussion

3.1. Crystal Structures and Morphologies of Samples

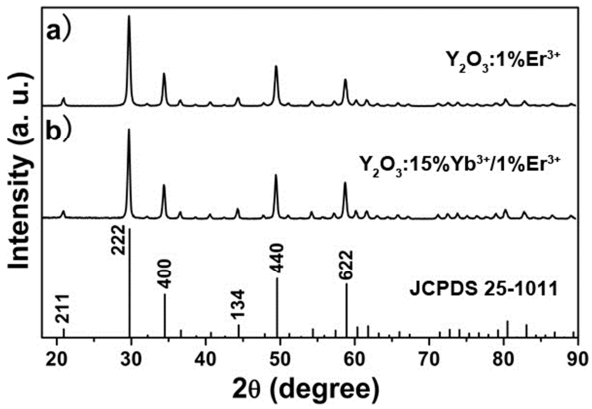

Figure 1. *XRD patterns of (a) Y_2O_3:1%Er^{3+} and (b) Y_2O_3:15% Yb^{3+}/1%Er^{3+}. The standard data for Y_2O_3 (JCPDS card 25-1011) is also presented in the figure for comparison.*

Figure 1 shows the XRD patterns of Y_2O_3:1%Er^{3+} and Y_2O_3:15%Yb^{3+}/1%Er^{3+} nanocrystals annealed at 800°C, respectively. All diffraction peaks can be readily indexed to pure cubic phase of Y_2O_3 [space group: *Ia3*(206)] according to the JCPDS file no. 25-1011. No additional peaks of other phases have been found, indicating that the Er^{3+} and Yb^{3+}/Er^{3+} ions are effectively built into the Y_2O_3 host lattice. The calculated lattice constants by using the Jade 5.0 program are that $a = b = c = 1.0616$ nm for Y_2O_3:1%Er^{3+} and $a = b = c = 1.0618$ nm for Y_2O_3:15%Yb^{3+}/1%Er^{3+}, both of which are compatible with the literature values from the standard card (1.0614 nm, JCPDS 25-1011). It is worth noting that when the Y^{3+} was substituted by the Yb^{3+}/Er^{3+} with bigger radius, the

corresponding lattice constants become a little bigger and the corresponding XRD peaks (for example, (222) peak) move to a lower degree [12]. In addition, high crystallinity can be obtained at a relatively low temperature. This is important for phosphors, since high crystallinity always means less traps and stronger luminescence.

The crystallite size of the samples can be estimated from the Scherrer equation, $D = 0.941\lambda/\beta\cos\theta$, where D is the average grain size, λ is the X-ray wavelength (0.15405 nm), and θ and β are the diffraction angle and full-width at half-maximum (fwhm, in radian) of an observed peak, respectively [13]. The strongest peak (222) at $2\theta = 29.76°$ was used to calculate the average crystallite size (D) of the Y_2O_3:Yb^{3+}/Er^{3+} particles. The estimated average crystallite size is about 23 nm.

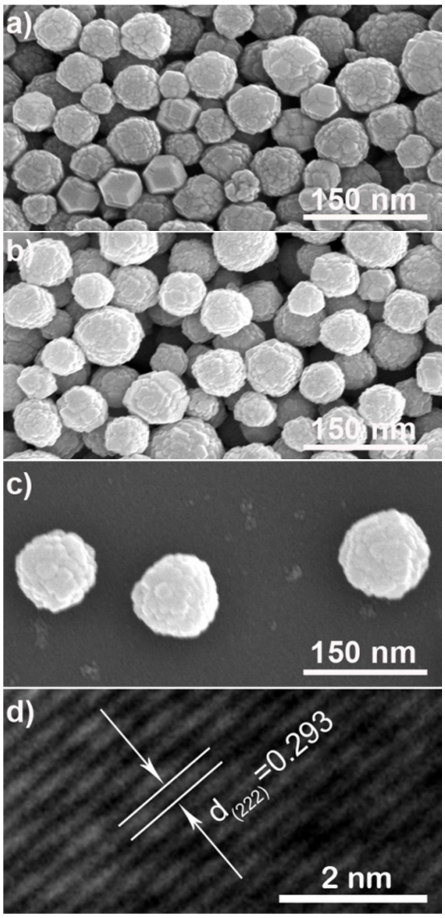

Figure 2. *SEM images of the hydrothermal precursor (a) and Y_2O_3:15% Yb^{3+}/1%Er^{3+} (b, c); HRTEM image of a part of one nanosphere (d).*

Figure 2a shows typical SEM images of hydrothermal precursors synthesized at 160°C. The SEM observations show that the precursors were composed of separated spheres with a mean diameter of about 80 nm because of isotropic growth caused by EG adsorption. After being annealed at 800°C, the obtained Y_2O_3:Yb^{3+}/Er^{3+} products kept the spherical shape of the hydrothermal precursors, but the diameter was reduced to about 75 nm (Figure 2b, c) due to the decomposition. The decrease in size from hydrothermal precursor to corresponding oxide through thermal decomposition is common for lanthanum compounds. The obtained Y_2O_3:Yb^{3+}/Er^{3+} spheres are smaller than the hydrothermal precursor spheres, which can be understood by the fact that the density of the former is higher than that of the latter [14]. In addition, the nanospheres of Y_2O_3:Yb^{3+}/Er^{3+} actually are composed of smaller grains with an average size of 25 nm. There is a small deviation in the estimated particle sizes by XRD and SEM analysis. Because smaller nanograins contribute more to the broadening of the diffraction peaks, the average nanocrystal size estimated from the Scherrer's equationis smaller than that determined from SEM technology in the case of Y_2O_3:Yb^{3+}/Er^{3+} nanospheres [15]. To further study the fine structure of the above nanospheres, transmission electron microscopy (TEM) was performed. The HRTEM image (Figure 2d) of a part of one nanosphere shows several lattice planes with good crystallinity. The lattice fringes show the imaging characteristics of the cubic Y_2O3 crystal, in which the d-spacing of 0.293 nm corresponding to the distance between the (222) planes.

3.2. Upconversion Photoluminescence Properties

Figure 3 shows the PL spectra of Y_2O_3:Yb^{3+}/Er^{3+} nanocrystals under 980 nm LD excitation. Figure 3a shows the bright green emission of Y_2O_3:1%Er^{3+} nanocrystals excited at 980 nm. Two primary bands in the green emission region maximized at 540 and 565 nm are assigned to Er^{3+} $^2H_{11/2} \rightarrow {}^4I_{15/2}$ and $^4S_{3/2} \rightarrow {}^4I_{15/2}$ transitions respectively, and a quite weak band appearing near 662 nm is ascribed to Er^{3+} $^4F_{9/2} \rightarrow {}^4I_{15/2}$ transition. However, the green emission of Y_2O_3:1%Er^{3+} nanocrystals changes greatly when Yb^{3+} was codoped with Er^{3+} in Y_2O_3 nanocrystals. The Y_2O_3:15%Yb^{3+}/1%Er^{3+} nanocrystals sample shows a strong red light under 980 nm LD excitation. Figure 3b shows the emission spectrum of Y_2O_3:15%Yb^{3+}/1%Er^{3+} nanocrystals, including mainly bright red emission of Er^{3+} near 662 nm corresponding to Er^{3+} $^4F_{9/2} \rightarrow {}^4I_{15/2}$ transition, together with the very weak emissions near 540 and 565 nm assigned to Er^{3+} $^2H_{11/2} \rightarrow {}^4I_{15/2}$ and $^4S_{3/2} \rightarrow {}^4I_{15/2}$ transitions respectively.

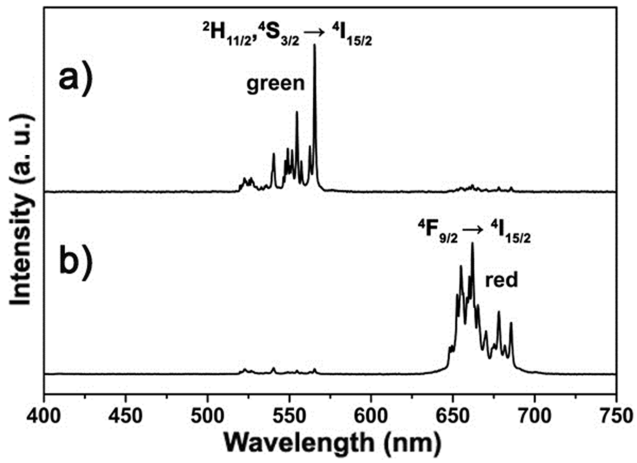

Figure 3. *Up-conversion PL emission spectra of Y_2O_3:Yb^{3+}/Er^{3+} nanocrystals under 980 nm LD excitation: (a) Y_2O_3:1% Er^{3+} and (b) Y_2O_3:15%Yb^{3+}/1%Er^{3+}.*

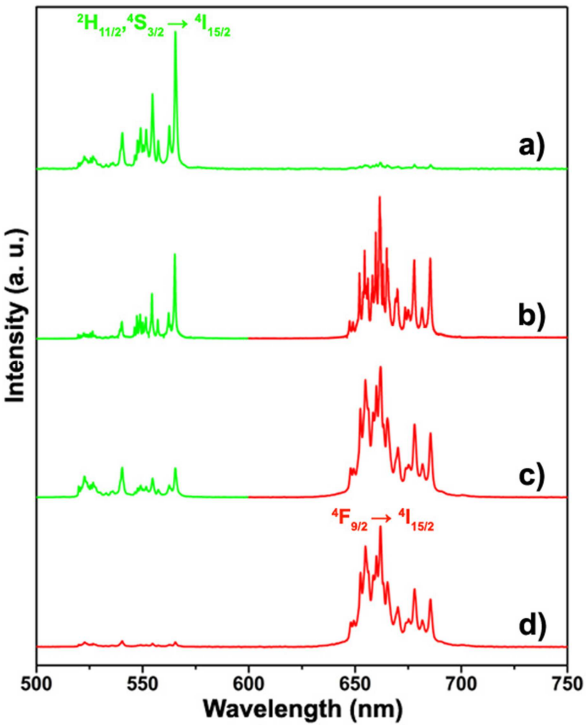

Figure 4. *Up-conversion PL emission spectra of different concentration of Yb^{3+} in 1%Er^{3+}-doped Y_2O_3 nanocrystals under 980 nm LD excitation: (a) Y_2O_3:1%Er^{3+}, (b) Y_2O_3:5%Yb^{3+}/1%Er^{3+}, (c) Y_2O_3:10%Yb^{3+}/1%Er^{3+}, (d) Y_2O_3:15%Yb^{3+}/1%Er^{3+}.*

It is well known that codoping can not only increase the efficiency of PL, but also induce up-conversion PL between the donor and acceptor ions in some cases [16]. In our present work, Yb^{3+} was chosen as the codopant with Er^{3+} because it possesses a large absorption cross-section at 980 nm, and energy transfer occurs as a result of the large spectral overlap between the Yb^{3+} emission $^2F_{5/2} \rightarrow {}^2F_{7/2}$ and the Er^{3+} absorption $^4I_{11/2} \leftarrow {}^4I_{15/2}$ bands. In addition, Yb^{3+} has a much longer excited-state lifetime [16]. The mechanism of the up-converted green emission of the Y_2O_3:1%Er^{3+} nanocrystals has been well established by others [17, 18]. The excitation wavelength from 980 nm LD matches the absorption transition between the ground state, $^4I_{15/2}$, and the excited level $^4I_{11/2}$ (GSA). After first-level excitation, the same wavelength laser pumps the excited atom from the $^4I_{11/2}$ to the $^4F_{7/2}$ level (ESA). Subsequent nonradiative relaxation populates the $^2H_{11/2}$,$^4S_{3/2}$ and the $^4F_{9/2}$ levels. Finally, radiant transitions from these levels yield the emissions at 540 and 565 nm ($^2H_{11/2}$,$^4S_{3/2} \rightarrow {}^4I_{15/2}$) (most strong) and at 662 nm ($^4F_{9/2} \rightarrow {}^4I_{15/2}$), respectively. For red light emission of the Y_2O_3:15%Yb^{3+}/1%Er^{3+} nanocrystals sample, the mechanism of up-conversion emission is predominantly due to the two-step ET from the excited Yb^{3+} to Er^{3+} and little contribution from Er^{3+} ground/excited-state absorption (GSA/ESA), because Yb^{3+} ions have a much larger absorption cross section and ion concentrations than that of Er^{3+} ions [19]. At first, Yb^{3+} ions are excited from $^2F_{7/2}$ to $^2F_{5/2}$ level by 980 nm laser, and then a excited Yb^{3+} transfer its energy to Er^{3+} ($^4I_{11/2}$). During the lifetime of the $^4I_{11/2}$ level, a second Yb^{3+} ion transfers its energy again, resulting in the population of the $^4F_{7/2}$ state of Er^{3+}. Relaxation from the $^4F_{7/2}$ state and some other energy transfer processes populate the $^2H_{11/2}$,$^4S_{3/2}$ and the $^4F_{9/2}$ states, which results in the observed emission spectra, namely, 662 nm corresponding to $^4F_{9/2} \rightarrow {}^4I_{15/2}$ (most strong) and 540/565 nm corresponding to $^2H_{11/2}$/$^4S_{3/2} \rightarrow {}^4I_{15/2}$.

Figure 4 shows the PL spectra of different concentration of Yb^{3+} in Er^{3+} doped Y_2O_3 nanocrystals under 980 nm LD excitation. Using a fixed Er^{3+} concentration (1 mol%) and upon variation of the Yb^{3+} concentration (from 0 to 15 mol%), it was found that the green emission intensity decreased while the red emission intensity increased (Figure 4). Such a result is also observed from Er^{3+} doped other oxides nanocrystals [20]. This case (the green emission decrease while the red emission enhancement) can be due to fewer Er^{3+} ions holding at the green emitting levels of $^2H_{11/2}$/$^4S_{3/2}$ and more Er^{3+} ions holding at the red emitting level of $^4F_{9/2}$ in nature. One of the most likely reasons is that introduction of an elevated amount of Yb^{3+} dopants in the Y_2O_3 host lattice would decrease $\cdots Yb^{3+} \cdots Er^{3+} \cdots$ interatomic distance and thus facilitate two energy back transfer process $^4S_{3/2}$ (Er^{3+}) + $^2F_{7/2}$ (Yb^{3+}) → $^4I_{13/2}$ (Er^{3+}) + $^2F_{5/2}$ (Yb^{3+}) and $^4F_{7/2}$ (Er^{3+}) + $^2F_{7/2}$ (Yb^{3+}) → $^4I_{11/2}$ (Er^{3+}) + $^2F_{5/2}$ (Yb^{3+}) efficiently, respectively. The former energy back transfer should subsequently suppress the population in excited levels of $^4S_{3/2}$($^2H_{11/2}$), resulting in the decrease of green ($^2H_{11/2}$/$^4S_{3/2} \rightarrow {}^4I_{15/2}$) light emission. At the same time, the energy back transfer leads to in the saturation of the $^4I_{13/2}$ (Er^{3+}) state and then excited Yb^{3+} ions transfer its energy to Er^{3+} ions through energy transfer process $^4I_{13/2}$ (Er^{3+}) + $^2F_{5/2}$ (Yb^{3+}) → $^4F_{9/2}$ (Er^{3+}) + $^2F_{7/2}$ (Yb^{3+}) which can directly populate the $^4F_{9/2}$ (Er^{3+}) level [21], producing the enhancement of red ($^4F_{9/2} \rightarrow {}^4I_{15/2}$) emission. In addition, the populated $^4I_{13/2}$ level can be excited to the $^4F_{9/2}$ red emitting level in Er^{3+} ions by cross relaxation process $^4I_{13/2}$ + $^4I_{11/2} \rightarrow {}^4F_{9/2}$ + $^4I_{15/2}$ possibly. The latter energy back transfer process should depopulate the excited $^4F_{7/2}$ (Er^{3+}) level at higher Yb^{3+} concentrations. This results in a smaller population of the $^2H_{11/2}$,$^4S_{3/2}$ green emitting levels and causes a decrease in the green emission intensity. Another possible route is the higher efficiency of the cross relaxation in Er^{3+} ions, i.e., $^4F_{7/2}$ + $^4I_{11/2} \rightarrow {}^4F_{9/2}$ + $^4F_{9/2}$, which also can directly populate the $^4F_{9/2}$ red emitting level and indirectly depopulate the $^2H_{11/2}$,$^4S_{3/2}$ green emitting levels [22, 23].

4. Conclusion

In summary, the fine, dispersed, and homogeneous nanosphere Y_2O_3:Yb^{3+}/Er^{3+} phosphors with dimension of about 75 nm were prepared by a simple hydrothermal method followed by a subsequent calcination process without using any template. In the hydrothermal process, stable spherical hydrothermal precursors were obtained because of the isotropic growth caused by EG adsorption. The subsequent calcination generated Y_2O_3:Yb^{3+}/Er^{3+} spheres with highly crystalline at the desired temperature. Under the excitation of 980-nm laser, the Y_2O_3:Yb^{3+}/Er^{3+} phosphors exhibit bright

upconversion photoluminescence from green to red with different Yb^{3+} content, which is easily observed by our naked eyes. The corresponding luminescent mechanisms have been discussed. Due to multicolor tunable luminescence, ideal spherical shape, and cheap materials of Y_2O_3 host, the as-prepared phosphors are potentially applied for color displays, back light, UC lasers, photonics, and biomedicine. Furthermore, this synthesis route may be of great significance in the preparation of other rare earth oxides spherical materials.

Acknowledgements

This project is financially supported by the National Undergraduate Training Program for Innovation and Entrepreneurship of Southwest University, China (201410635027).

References

[1] Y. Zhang, W. T. Gong, J. J. Yu, Z. Y. Cheng, G. L. Ning, *RSC Adv.* 2016, *6*, 30886.

[2] X. He, B. Yan, *J. Mater. Chem. C*, 2014, *2*, 2368.

[3] L. Zhou, L. Yuan, X. J. Zhou, S. S. Hu, Y. Luo, J. Yang, *Chemistry Select*, 2016, *1*, 1848.

[4] S. H. Cho, S. H. Kwon, J. S. Yoo, C. W. Oh, J. D. Lee, K. J. Hong, S. J. Kwon, *J. Electrochem. Soc.*, 2000, 147, 3143.

[5] H. Wang, C. K. Lin, X. M. Liu, J. Lin, *Appl. Phys. Lett.*, 2005, 87, 181907.

[6] B. Alken, W. P. Hsu, E. Matijevic, *J. Am. Ceram. Soc.*, 1988, 71, 845.

[7] Z. H. Xu, Y. Gao, T. Liu, L. M. Wang, S. S. Bian, J. Lin, *J. Mater. Chem.*, 2012, 22, 21695.

[8] M. S. Palmer, M. Neurock, M. M. Olken, *J. Am. Chem. Soc*., 2002, 124, 8452.

[9] J. A. Nelson, E. L. Brant, M. J. Wagner, *Chem. Mater.*, 2003, 15, 688.

[10] S. S. Hu, H. G. Zhang, J. Yang, Z. H. Qiao, *J. Nanosci. Nanotechnol.* 2014, *14*, 3853.

[11] X. Bai, H. W. Song, L. X. Yu, L. M. Yang, Z. X. Liu, G. H. Pan, S. Z. Lu, X. G. Ren, Y. Q. Lei, L. B. Fan, *J. Phys. Chem. B*, 2005, 109, 15236.

[12] J. Yang, C. M. Zhang, C. X. Li, Y. N. Yu, J. Lin, Inorg. Chem., 2008, 47, 7262.

[13] Y. W. Zhang, S. Jin, S. J. Tian, G. B. Li, T. Jia, C. S. Liao, C. H. Yan, Chem. Mater. 2001, 13, 372.

[14] A. W. Xu, Y. P. Fang, L. P. You, and H. Q. Liu, *J. Am. Chem. Soc*, 2003, 125, 1494.

[15] W. B. Pei, B. Chen, L. L. Wang, J. S. Wu, X. Teng, R. Lau, L. Huang, W. Huang, *Nanoscale*, 2015, *7*, 4048.

[16] G. K. Das, T. Y. Tan, *J. Phys. Chem. C* 2008, *112*, 11211.

[17] D. Matsuura, *Appl. Phys. Lett.* 2002, *81*, 4526.

[18] A. Patra, C. S. Friend, R. Kapoor, P. N. Prasad, *J. Phys. Chem. B* 2002, *106,* 1909.

[19] S. Sivakumar, F. C. J. M. van Veggel, M. Raudsepp, *J. Am. Chem. Soc.* 2005, *127*, 12464.

[20] X. Bai, H. W. Song, G. H. Pan, Y. Q. Lei, T. Wang, X. G. Ren, S. Z. Lu, B. Dong, Q. L. Dai, L. B. Fan, *J. Phys. Chem. C*, 2007, *111*, 13611.

[21] G. Y. Chen, Y. G. Zhang, G. Somesfalen, Z. G. Zhang, Q. Sun, F. P. Wang, *Appl. Phys. Lett.* 2006, *89*, 163105.

[22] F. Vetrone, J. C. Boyer, J. A. Capobianco, *J. Appl. Phys.* 2004, *96*, 661.

[23] J. J. Cao, L. Yuan, J. F. Tang, X. J. Zhou, J. Yang, *CrystEngComm*, 2016, *18*, 5940.